AGU PUBLICATIONS

JGR

Journal of Geophysical Research: Planets

RESEARCH ARTICLE
10.1002/2015JE004828

Key Points:
- MESSSENGER data reveal stratigraphic relations between lobate scarps and craters
- Such relations constrain the timing and duration of Mercury's global contraction
- Global contraction deformed Mercury's surface over much of the last 3–4 Gyr

Correspondence to:
M. E. Banks,
banks@psi.edu

Citation:
Banks, M. E., Z. Xiao, T. R. Watters, R. G. Strom, S. E. Braden, C. R. Chapman, S. C. Solomon, C. Klimczak, and P. K. Byrne (2015), Duration of activity on lobate-scarp thrust faults on Mercury, *J. Geophys. Res. Planets*, *120*, 1751–1762, doi:10.1002/2015JE004828.

Received 7 APR 2015
Accepted 28 SEP 2015
Accepted article online 2 OCT 2015
Published online 7 NOV 2015

Duration of activity on lobate-scarp thrust faults on Mercury

Maria E. Banks[1,2], Zhiyong Xiao[3,4,5], Thomas R. Watters[1], Robert G. Strom[3], Sarah E. Braden[6], Clark R. Chapman[7], Sean C. Solomon[8,9], Christian Klimczak[9,10], and Paul K. Byrne[9,11]

[1]Center for Earth and Planetary Studies, National Air and Space Museum, Smithsonian Institution, Washington, District of Columbia, USA, [2]Planetary Science Institute, Tucson, Arizona, USA, [3]Lunar and Planetary Laboratory, University of Arizona, Tucson, Arizona, USA, [4]School of Earth Sciences, China University of Geosciences, Wuhan, Hubei, China, [5]Centre for Earth Evolution and Dynamics, University of Oslo, Oslo, Norway, [6]School of Earth and Space Exploration, Arizona State University, Tempe, Arizona, USA, [7]Department of Space Studies, Southwest Research Institute, Boulder, Colorado, USA, [8]Lamont-Doherty Earth Observatory, Columbia University, Palisades, New York, USA, [9]Department of Terrestrial Magnetism, Carnegie Institution of Washington, Washington, District of Columbia, USA, [10]Department of Geology, University of Georgia, Athens, Georgia, USA, [11]Lunar and Planetary Institute, Universities Space Research Association, Houston, Texas, USA

Abstract Lobate scarps, landforms interpreted as the surface manifestation of thrust faults, are widely distributed across Mercury and preserve a record of its history of crustal deformation. Their formation is primarily attributed to the accommodation of horizontal shortening of Mercury's lithosphere in response to cooling and contraction of the planet's interior. Analyses of images acquired by the Mariner 10 and MErcury Surface, Space ENvironment, GEochemistry, and Ranging (MESSENGER) spacecraft during flybys of Mercury showed that thrust faults were active at least as far back in time as near the end of emplacement of the largest expanses of smooth plains. However, the full temporal extent of thrust fault activity on Mercury, particularly the duration of this activity following smooth plains emplacement, remained poorly constrained. Orbital images from the MESSENGER spacecraft reveal previously unrecognized stratigraphic relations between lobate scarps and impact craters of differing ages and degradation states. Analysis of these stratigraphic relations indicates that contraction has been a widespread and long-lived process on the surface of Mercury. Thrust fault activity had initiated by a time near the end of the late heavy bombardment of the inner solar system and continued through much or all of Mercury's subsequent history. Such deformation likely resulted from the continuing secular cooling of Mercury's interior.

1. Introduction

1.1. Background

Mercury's tectonic history has been dominated by contraction, as evident from the many landforms interpreted as surface manifestations of thrust faults, including lobate scarps, high-relief ridges, and wrinkle ridges [e.g., *Strom et al.*, 1975; *Melosh and McKinnon*, 1988; *Watters et al.*, 1998, 2002, 2004, 2009a, 2009b]. Here we focus on Mercury's lobate scarps, which are interpreted as expressions of surface-breaking thrust faults (for example, see Figure 1). Lobate scarps can extend for more than 500 km in length and display up to ~3 km of relief [e.g., *Strom et al.*, 1975; *Strom and Sprague*, 2003; *Solomon et al.*, 2008; *Watters et al.*, 1998, 2013; *Byrne et al.*, 2014]. Their scale, widespread distribution, and broad range of orientations have been attributed primarily to shortening of the lithosphere in response to cooling and contraction of the planetary interior [e.g., *Strom et al.*, 1975; *Watters et al.*, 1998; *Strom and Sprague*, 2003; *Solomon et al.*, 2008; *Watters and Nimmo*, 2010].

The timing and extent of Mercury's contraction in radius are key constraints on interior thermal history models [e.g., *Hauck et al.*, 2004; *Solomon et al.*, 2008; *Tosi et al.*, 2013]. In addition, because a stress state in which the two most compressive principal stresses are horizontal serves to inhibit magma ascent [e.g., *Solomon*, 1978], information on the onset and duration of such a stress state is important for interpreting the ages and distribution of volcanic deposits on Mercury.

Analyses of images acquired by the Mariner 10 and the MErcury Surface, Space ENvironment, GEochemistry, and Ranging (MESSENGER) spacecraft during flybys of Mercury showed that the planet's lobate scarps deform all major geologic units, including heavily cratered terrain, intercrater plains, and smooth plains. Moreover, these analyses suggested that some thrust faulting initiated near the end of the emplacement

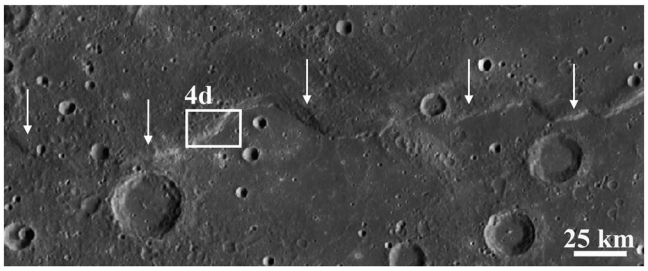

Figure 1. Calypso Rupes (white arrows), one of Mercury's prominent lobate scarps. The white box marks the location of Figure 4d. In this portion of an MDIS mosaic, and in all other images in this paper, north is up and the image is shown in a sinusoidal projection. The mosaic is centered at ~19.0°N, 41.5°E.

of the youngest major smooth plains deposits and continued for some time thereafter [e.g., *Strom et al.*, 1975; *Spudis and Guest*, 1988; *Melosh and McKinnon*, 1988; *Strom and Sprague*, 2003; *Solomon et al.*, 2008; *Watters et al.*, 2004, 2009a, 2009b]. No widespread evidence of embayment of lobate scarps by earlier intercrater plains material has been documented [*Watters et al.*, 2004, 2009b], although one possible example of partial embayment of a lobate scarp by younger smooth plains has been identified [*Watters et al.*, 2009b]. However, the full temporal extent of thrust fault activity on Mercury could not be constrained by these analyses, particularly the duration of lobate scarp activity subsequent to the time of youngest major smooth plains emplacement.

In this paper we use images and image mosaics of Mercury acquired from orbit by MESSENGER's Mercury Dual Imaging System (MDIS) [*Hawkins et al.*, 2007] to identify stratigraphic relations between lobate scarps and impact craters of different ages and states of preservation. From a global assessment of those relations, we address the duration of thrust fault activity on Mercury. Before discussing those relations, we present brief overviews of Mercury's time-stratigraphic systems for assigning relative ages of geological units and features and standard morphological classification criteria for assessing the relative ages of impact craters.

1.2. Mercury's Time-Stratigraphic System

On the basis of morphologically distinct basin and crater deposits, *Spudis and Guest* [1988] subdivided Mercury's surface units into five time-stratigraphic systems. Approximate age limits were suggested for these systems by *Spudis and Guest* [1988] on the basis of the lunar impact-flux history of *Shoemaker and Hackman* [1962]. From oldest to youngest, these systems are the pre-Tolstojan (> ~4.0 Ga), Tolstojan (~4.0 to 3.9 Ga), Calorian (~3.9 to ~3.5–3.0 Ga), Mansurian (~3.5–3.0 to 1.0 Ga), and Kuiperian (< ~1.0 Ga) [*Spudis and Guest*, 1988].

The pre-Tolstojan includes extensive intercrater plains materials and ancient multi-ring basins. The deposits of the Tolstoj basin define the base of the Tolstojan system, which also includes the oldest smooth plains materials (i.e., those with the highest areal densities of superposed impact craters) [*Spudis and Guest*, 1988]. The base of the Calorian system is defined by the Caloris basin, which is thought to date from near the end of the late heavy bombardment (LHB) of the inner Solar System [e.g., *Strom et al.*, 2005]. The Calorian system includes the youngest widespread smooth volcanic plains deposits [*Spudis and Guest*, 1988].

A recent crater production function and inner solar system chronology [*Marchi et al.*, 2009] indicate that the oldest surfaces on Mercury date from about 4.0–4.1 Ga during the LHB [*Marchi et al.*, 2013] and correspond approximately to the Pre-Tolstojan and Tolstojan systems [*Spudis and Guest*, 1988]. Widespread smooth volcanic plains were emplaced by about 3.55–3.8 Ga [*Marchi et al.*, 2013], at the end of the Calorian system [*Spudis and Guest*, 1988]. Age estimates from crater production functions are model dependent, however, and thus carry systematic uncertainties that are difficult to ascertain.

The Calorian system is followed chronologically by the Mansurian and Kuiperian systems, analogous to but not well time-correlated with the lunar Eratosthenian and Copernican systems, respectively [*Spudis and Guest*, 1988; *Denevi and Robinson*, 2008; *Braden and Robinson*, 2013]. These systems are defined by the craters Mansur and Kuiper, respectively, and include primarily impact crater deposits. The Mansurian includes slightly degraded but still relatively fresh craters and only minor plains materials confined to basin and crater floors. Mansurian craters do not have bright ray systems, but they have crisp morphologies and fine-scale structures (see further discussion below) [*Spudis and Guest*, 1988]. The base of the Kuiperian system is loosely defined by the oldest fresh craters with bright ray systems and high-reflectance ejecta blankets, typified by the deposits of Kuiper crater [*Spudis and Guest*, 1988]. *Spudis and Guest* [1988] estimated the base of the Kuiperian at approximately 1 Ga, corresponding approximately to the Copernican period on the Moon

(~800 ± 15 Ma or younger) [*Stöffler and Ryder*, 2001]. However, model ages obtained with more recent crater production functions [*Marchi et al.*, 2009; *Le Feuvre and Wieczorek*, 2011] suggest that the average age of the population of rayed craters on Mercury may be less than ~250 Myr [*Xiao et al.*, 2012]. A younger age for Mercury's rayed craters is also supported by the finding of *Braden and Robinson* [2013] that rates of optical maturation are up to four times higher on Mercury than on the Moon.

1.3. Crater Morphological States

Impact craters form continuously on planetary and satellite surfaces. They are progressively eroded or degraded by subsequent impacts and mass wasting, and, as a result, craters of different ages exhibit different morphological states (Figure 2). Degradation rates on Mercury are expected to be higher than those on the Moon. The rate of erosion from subsequent cratering in particular is higher on Mercury because of its greater impact flux and higher mean impact velocities [*Gault et al.*, 1975; *Cintala*, 1992; *Le Feuvre and Wieczorek*, 2011; *Domingue et al.*, 2014; *Kreslavsky et al.*, 2014]. Moreover, because of Mercury's higher surface gravitational acceleration, material ejected to a given range from a primary crater impacts the surface at a greater velocity [*Scott*, 1977; *Xiao et al.*, 2014] and thus with greater erosive power [*Spudis and Guest*, 1988]. Craters of similar sizes and states of degradation should thus be younger on Mercury than on the Moon.

The degree of degradation or morphological crispness of a crater provides an indication of the crater's relative age [e.g., *Pohn and Offield*, 1970; *Trask*, 1971, 1975; *Moore et al.*, 1980]. Fresh or young craters are characterized by crisp morphologies with well-preserved rims, few or no superposed craters, continuous ejecta with radial lineaments, and well-defined secondary craters [*Arthur et al.*, 1963; *Leake*, 1982; *Spudis and Guest*, 1988] (Figures 2a–2c). All fresh craters on Mercury are interpreted to have formed from impact events occurring after the LHB and the Calorian system. Thus, all fresh craters are considered Mansurian in age or younger [*Spudis and Guest*, 1988]. Mercury's youngest craters commonly have bright ray systems and high-reflectance ejecta blankets (Figure 2a). As discussed above, all rayed craters are Kuiperian. Once thought to be as old as ~1 Gyr [*Spudis and Guest*, 1988], Kuiperian craters are now estimated to be potentially younger than ~250 Myr [*Marchi et al.*, 2009; *Le Feuvre and Wieczorek*, 2011; *Xiao et al.*, 2012; *Braden and Robinson*, 2013].

Trask [1971] and *Moore et al.* [1980] showed that lunar craters that are ≤3 km in diameter, and "relatively fresh," with rims that are sharp to only slightly or moderately subdued (including craters that lack rays), are interpreted to be Copernican in age (see images in Figure 2 of *Trask* [1971] and Figure 4 of *Moore et al.* [1980]). Small craters degrade and disappear faster than larger craters. Lunar craters of this small size that formed prior to the Copernican system appear more heavily degraded [e.g., *Arthur et al.*, 1963; *Trask*, 1971; *Moore et al.*, 1980]. On Mercury, by analogy, small (≤3 km in diameter) and relatively fresh craters (those with states of degradation comparable with those of small lunar Copernican craters) are interpreted to be Kuiperian in age. Higher degradation rates expected for Mercury compared with the Moon reinforce this interpretation.

Impact craters greater than ~3 km in diameter that no longer have bright rays and ejecta but still retain the crisp characteristics of fresh craters (described above) are considered Mansurian [*Spudis and Guest*, 1988] (Figure 2c). Craters interpreted as Calorian in age have several superposed craters and are moderately degraded with subdued ejecta blankets and moderately subdued and rounded rim crests (Figure 2d). Tolstojan craters have many superposed craters, greater degrees of degradation, and heavily rounded rim crests, indistinct ejecta blankets, and partially infilled crater floors (Figure 2e). The most heavily degraded craters are considered pre-Tolstojan and are often shallow depressions that lack a well-defined rim and have abundant superposed craters (Figure 2f) [e.g., *Pohn and Offield*, 1970; *Trask*, 1971, 1975; *Moore et al.*, 1980; *Spudis and Guest*, 1988]. Special care was taken when evaluating the degradation state of smaller craters (particularly those < ~10 km in diameter, because smaller craters degrade faster than larger craters), as well as with craters located near younger impacts sufficiently large to have contributed superposing secondary craters and/or ejecta material that might make the crater under evaluation appear more degraded than others of comparable age. In most instances, craters could be classified clearly into one of the categories above. In the rare instances when crater degradation states could not be confidently assessed, the ambiguous examples were not considered further in the analysis.

2. Methodology and Data

We make use of stratigraphic relations between lobate scarps and impact craters to estimate the age of the last detectable activity on individual segments of the scarp-associated faults. For example, a crater that is cut or

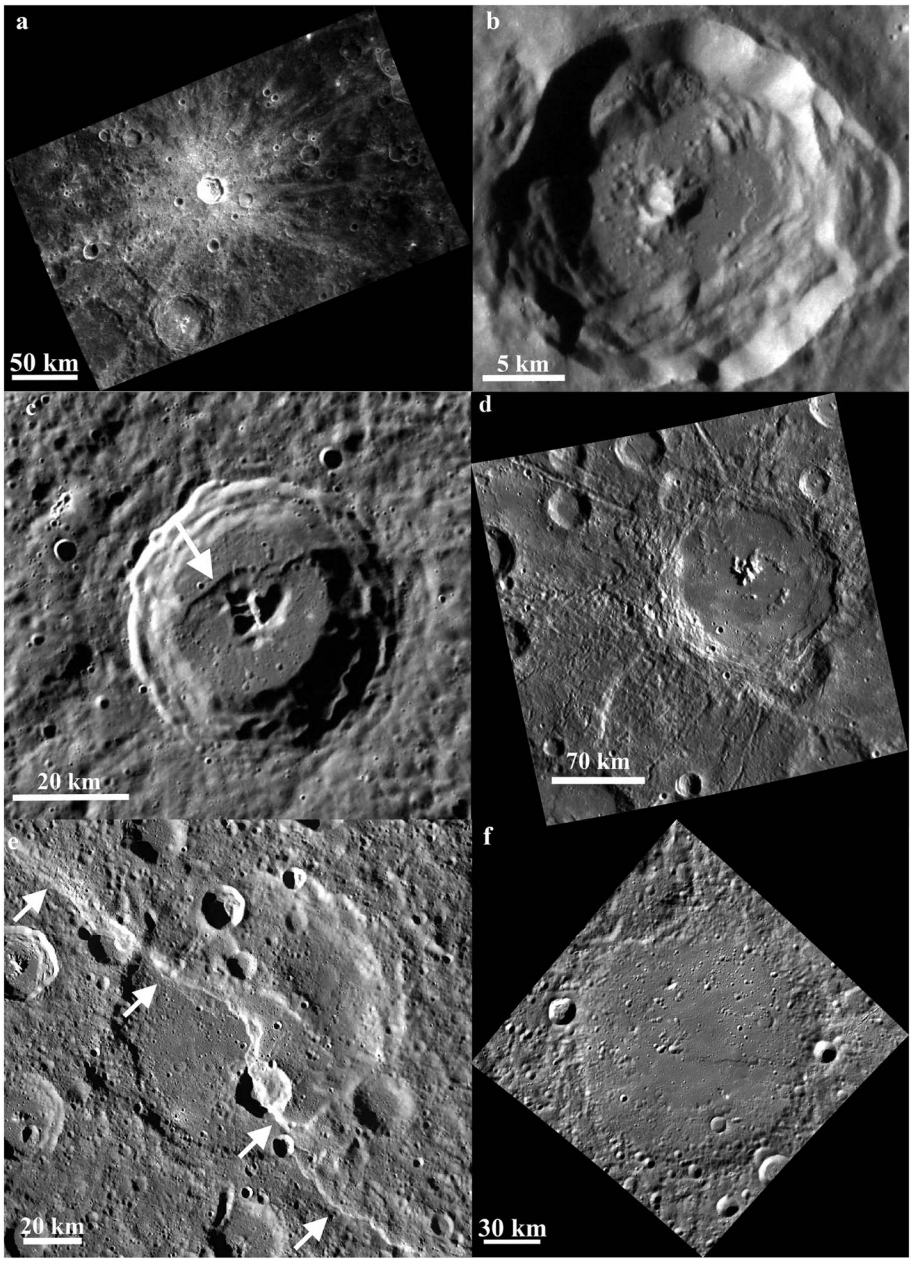

Figure 2. Impact craters exhibiting a range of degradation states, with sharp to indistinct morphologies, sampled from each of Mercury's stratigraphic systems. (a) Snorri, a Kuiperian rayed crater (centered at 9.4°S, 277.1°E; MDIS image EN0227045180M). (b) Close-up view of a Kuiperian rayed crater (9.5°S, 298.5°E; MDIS image EN0244057217M). (c) Mansurian crater crosscut by a lobate scarp (white arrow) (68.5°N, 181.5°E; MDIS image EW0213416030G). This crater is morphologically crisp, similar to fresh Kuiperian craters, but no longer has a bright ray system. (d) Joplin, a Calorian crater (38.9°S, 26.5°E; MDIS image EN0220021767M). (e) Duccio, a Tolstojan crater (58.0°N, 307.5°E; MDIS mosaic). This large crater in the center of the image, as well as several smaller surrounding craters, is crosscut by the lobate scarp (white arrows) Carnegie Rupes. (f) Botticelli, a pre-Tolstojan crater (63.6°N, 247.7°E; MDIS image EW0211981739G).

deformed by a scarp indicates that slip occurred on the underlying fault since the formation of the crater. In contrast, an undisturbed crater that superposes a scarp indicates that there has been no detectable slip on that fault segment since the impact (see further discussion in section 4). In some instances, of course, stratigraphic relations are ambiguous, and the relative age of scarp activity and crater formation cannot be clearly determined.

To ascertain such stratigraphic relations we examined MDIS monochrome images (with pixel scales as small as 10 m) as well as global mosaics (with average pixel scales of 250 m). With those images we identified

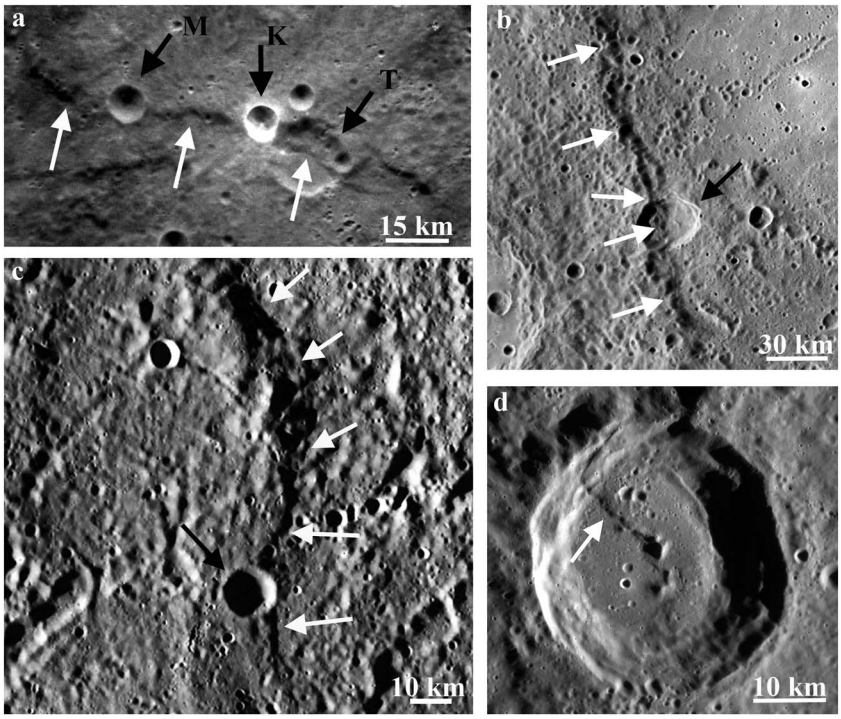

Figure 3. Stratigraphic relations between lobate scarps and Tolstojan, Calorian, and Mansurian craters. (a) Lobate scarp (white arrows) crosscutting a degraded Tolstojan crater (black arrow labeled "T") but superposed by a Mansurian crater (black arrow labeled "M") and a Kuiperian crater with faint rays (black arrow labeled "K"; 35.8°S, 186.2°E; MDIS image EN0245615161M). (b) Lobate scarp (white arrows) crosscutting the rim and floor of a Calorian crater with moderately degraded and subdued morphology (2.6°S, 320.4°E; MDIS image EW0212983120G). (c) Endeavour Rupes (white arrows) superposed by a Calorian crater (black arrow; 33.4°N, 327.7°E; MDIS image EW0228327929G). (d) Lobate scarp (white arrow) crosscutting a Mansurian crater (11.3°N, 0.0°E; MDIS image EN1015163976M).

impact craters that coincide spatially with segments of lobate scarps and analyzed the degree of degradation of those craters and evidence for post-impact activity on the thrust faults underlying these associated scarps. Approximately 400 lobate scarps were examined in this study, including all major scarps at least 100 km in length mapped by *Byrne et al.* [2014] and *Watters et al.* [2013, 2015b]. We systematically analyzed images of those scarps for crosscutting relations with impact craters of all resolvable sizes (typically $\geq$1 km in diameter) and degradation states. In addition, segments of lobate scarps that coincide spatially with Mansurian craters from the data set of *Braden and Robinson* [2013] and with all Kuiperian craters from the data sets of *Xiao et al.* [2012] and *Braden and Robinson* [2013] were included.

3. Results

On the basis of the time-stratigraphic system to which impact craters coinciding spatially with lobate scarp segments were assigned, we can make a number of general statements regarding the fraction of situations for which activity on the thrust faults underlying scarp segments either appears to have ceased prior to, or evidently continued after, the formation of craters of a given relative age.

Nearly all (~90%) of the lobate scarp segments examined in this study coincide spatially with Tolstojan and pre-Tolstojan craters. Importantly, all of the scarps collocated with craters in this age group crosscut and deform the associated craters. Examples of these relations can be seen in Figures 2e and 3a. There were no examples found in which a lobate scarp is superposed by an undeformed crater interpreted as Tolstojan or pre-Tolstojan in age.

About 65% of the scarp segments examined in this study coincide spatially with Calorian craters. Of the scarp segments collocated with Calorian craters, ~85% crosscut and deform the associated craters (Figure 3b), whereas ~15% are superposed by undeformed Calorian craters (Figure 3c).

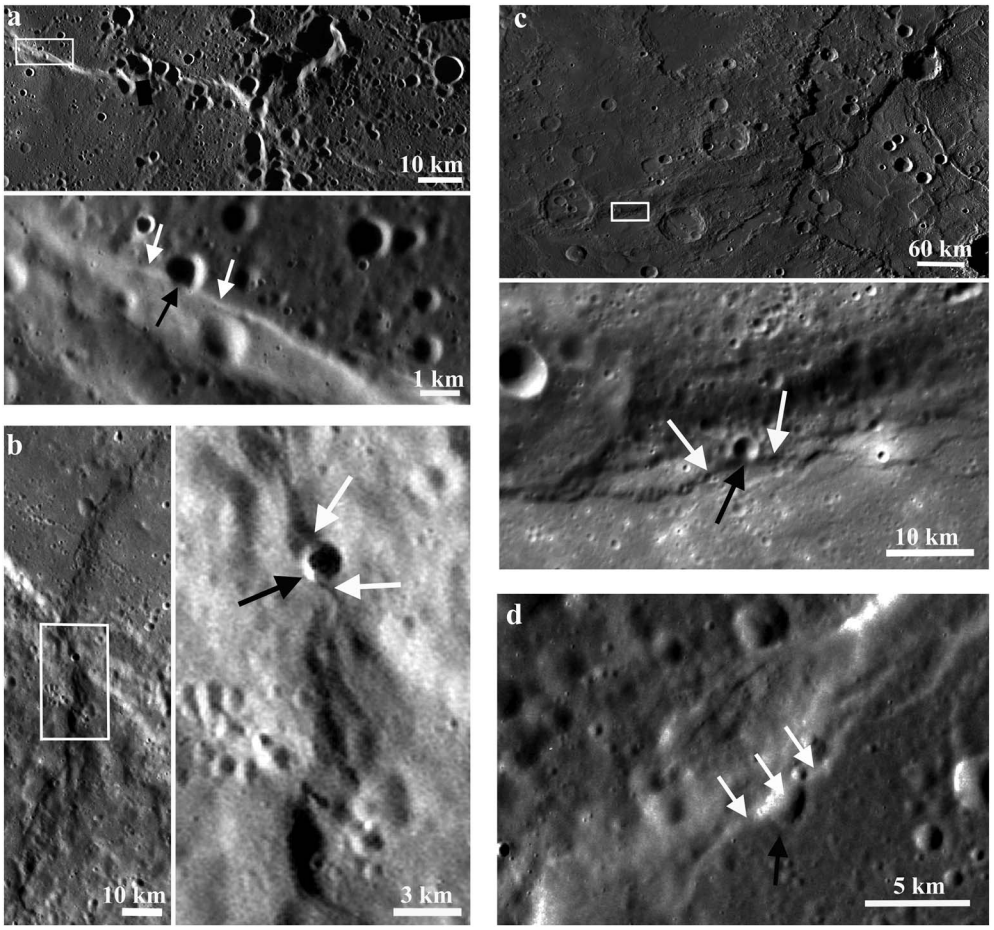

Figure 4. Evidence of thrust-fault activity in the Kuiperian. (a) Context (top panel, MDIS mosaic) and close-up (lower panel, MDIS image EN0239330240M) views of a lobate scarp (white arrows) crosscutting a small crater (black arrow, 44.8°N, 77.2°E) ~1 km in diameter. The crater is located atop the scarp, and the southern rim has been cut by the scarp face. (b) Context (left panel, MDIS mosaic) and close-up (right panel, MDIS image EN0235339992M) views of a crosscut ~2.8 km diameter crater (black arrow, 29.5°S, 30.0°E). The southern rim and likely the northern rim of this crater (white arrows) are cut by a lobate scarp. (c) Context (upper panel, MDIS mosaic) and close-up (lower panel, MDIS image EN0252267858M) views of Enterprise Rupes (white arrows) cutting a small crater ~2.7 km in diameter (black arrow, 37.85°S, 70.85°E). (d) Close-up view (MDIS image EN0250131823M) of Calypso Rupes (white arrows) where it cuts and deforms a crater with a diameter of ~2.2 km (black arrow, 19.2°N, 40.1°E). A context view of Calypso Rupes is seen in Figure 1. White boxes in the context views indicate the locations of the associated close-up views.

Approximately half of the scarp segments analyzed in this study coincide spatially with Mansurian craters. Of these segments, the majority (~75%) are superposed by the associated craters (Figure 3a), but in ~25% of the cases the scarps deform Mansurian craters (Figures 2c and 3d).

About ~20% of the analyzed scarp segments appear to coincide spatially with Kuiperian rayed craters or their associated secondary craters. For about half of these examples, no stratigraphic relation could be clearly discerned from the available images because of resolution or lighting conditions. For the remaining examples, the stratigraphic relation could be determined clearly, and in all such cases the scarp is superposed by the rayed crater or its associated secondary craters (Figure 3a).

MDIS orbital images show relatively fresh craters <3 km in diameter that coincide with the edges of the faces of some lobate scarps, a geometry that permits the stratigraphic relation between the scarp and the small crater to be assessed (Figure 4). Nearly all scarp segments are superposed by small fresh craters somewhere along their extent, although not always directly on the scarp face. About 100 small, fresh, and undeformed craters have been identified that are directly superposed on a scarp face and for which a clear stratigraphic relation could be determined. At least 15 small and relatively fresh craters are also seen to be crosscut or

modified by movement along the scarp. Four examples of these craters are shown in Figure 4. At the resolution of available images with a sufficiently low incidence angle for observing crater rays, no distinct rays are observed to be associated with these craters. Nonetheless, as discussed above, small craters (<3 km in diameter) with crisp to only slightly or moderately subdued morphologies are categorized as Copernican in age on the Moon and are interpreted here to be Kuiperian in age [see also *Trask*, 1971; *Gault et al.*, 1975; *Scott*, 1977; *Moore et al.*, 1980; *Spudis and Guest*, 1988; *Cintala*, 1992; *Le Feuvre and Wieczorek*, 2011; *Domingue et al.*, 2014].

For example, a segment of a scarp located near the southern edge of Mercury's northern smooth plains and between Copland (37.6°N, 73.1°E) and Rustaveli (52.4°N, 82.8°E) craters crosscuts a Kuiperian crater ~1 km in diameter (Figure 4a). Another example, shown in Figure 4b, is of a lobate scarp, located in the southern hemisphere northwest of Joplin crater (38.4°S, 25.6°E), that cuts the southern rim, and also likely the northern rim, of a crater ~2.8 km in diameter. Additional examples of relatively fresh craters with diameters of ~2.7 and ~2.2 km, respectively, that have been cut and deformed by lobate scarp segments are shown in Figures 4c and 4d. All of these examples suggest that activity on thrust faults underlying some lobate scarp segments occurred during the Kuiperian.

4. Discussion

Observations of impact craters crosscut by lobate scarps indicate that the most recent slip on the associated fault segment occurred at some time after the formation of the crater. This situation does not typically provide clear information on whether the scarp existed prior to the impact or when local fault activity initiated or ceased. It simply indicates that slip occurred on that particular fault segment following the impact and that such activity could still be ongoing. Conversely, observations of undeformed craters superposed on lobate scarps indicate that the formation of the scarp and initiation of slip on the associated thrust fault segment predated the impact and that no detectable displacement postdated the impact. However, apparent inactivity on the fault segment underlying the superposed section of scarp does not necessarily indicate inactivity along the entire length of the scarp. Moreover, the formation of the impact crater may have modified the stress field in the immediate vicinity of the crater by the release of preexisting stress and the formation of a damage zone [e.g., *Collins et al.*, 2004; *Senft and Stewart*, 2007; *Freed et al.*, 2009], thereby delaying the buildup of stress from further global contraction to levels capable of triggering local fault activity. Thus, for the purposes of this study, scarps superposed by undeformed craters constrain the initiation of shortening to a time before the crater-forming impact, and craters crosscut by scarps constrain the age of at least the most recent local shortening of the crust to a time after the crater-forming impact. These observations together provide insight into the duration of Mercury's tectonic activity. The time-dependent rate of global contraction through Mercury's geologic history, however, cannot be reliably constrained with these methods.

Crosscut and deformed Tolstojan and pre-Tolstojan craters indicate that the most recent activity along thrust faults associated with the transecting scarp segments postdated the Tolstojan or Pre-Tolstojan systems. These observations do not tell us whether the scarps in question formed before the Tolstojan system, but only that the thrust faults underlying all scarps examined in this study either formed or continued to be active subsequent to that period. It is important to note that any record of crustal deformation during the LHB is unlikely to have been preserved, so there is an inevitable bias against the detection of thrust fault activity prior to the end of the LHB.

Crosscut Calorian craters indicate that the most recent activity on the faults underlying the crosscutting scarp segments occurred toward the end of, or after, the Calorian system. However, the small fraction (~15%) of scarp segments superposed by Calorian craters show that some scarps had formed and their underlying thrust faults were active within or prior to the Calorian system. Together these observations support the interpretation that shortening of Mercury's surface had initiated on at least a regional scale prior to or during the Calorian (~3.55–3.8 Ga), a time interval during which the major expanses of smooth plains were emplaced [e.g., *Denevi et al.*, 2013].

Undeformed Mansurian craters that superpose lobate scarps indicate that all detectable activity on the underlying fault segments occurred prior to, or near the beginning of, the Mansurian system. Mansurian craters crosscut by scarps, in contrast, show that the faults underlying these scarp segments continued to be active during or more recently than the Mansurian system. For the scarps in this study for which stratigraphic

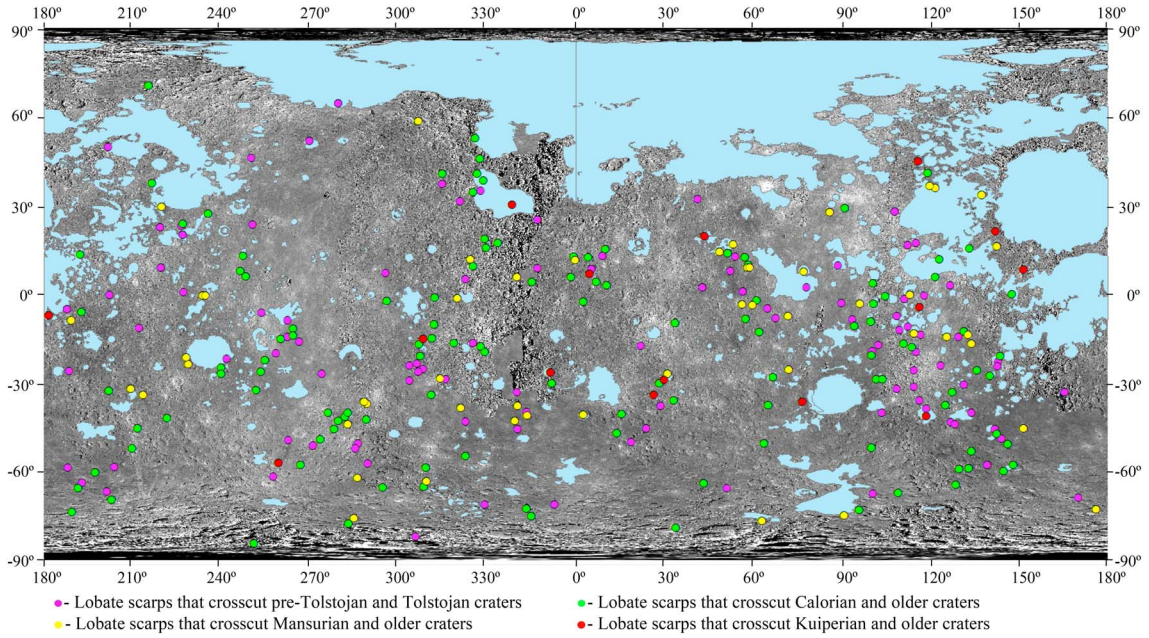

Figure 5. Locations of lobate scarp segments that coincide with impact craters, categorized by the youngest impact craters that are crosscut and deformed by the fault underlying the scarp. Scarp segments that crosscut only Tolstojan and pre-Tolstojan craters are represented by purple dots, scarp segments that crosscut Calorian and older craters by green dots, scarp segments that crosscut Mansurian and older craters by yellow dots, and scarp segments that crosscut Kuiperian craters <3 km in diameter and older craters by red dots. Only examples of crosscutting relationships that could be clearly discerned in available images are included. The background image is an MDIS monochrome map in equirectangular projection. Smooth plains units [*Denevi et al.*, 2013] are shown in light blue.

relations can be discerned between both degraded older (Calorian and/or older) and less degraded younger (Mansurian and/or Kuiperian) craters (~250 scarp segments), all of these scarps crosscut or deform the older degraded craters, and the majority (~80%) are superposed by the younger Mansurian and/or Kuiperian craters (Figure 3a). These observations support the inference that slip had already initiated along many thrust fault segments by the late Calorian to early or mid Mansurian, although it is difficult to quantify the amount of activity on the faults over earlier time intervals as the structures may have been active over extended periods.

Scarp segments superposed by rayed craters or their associated secondary craters must have formed, and the most recent detectable activity on the underlying faults must have ceased, prior to the early Kuiperian system (Figure 3a). However, shortening during the Kuiperian is suggested in those locations where small, relatively fresh craters (<3 km in diameter) are transected or modified by movement on the face of some scarp segments (Figure 4). Because of the small scale of these craters and the limits of the spatial resolution of the images, it is often difficult to determine clearly the precise degradation state of such a small transected crater. In some instances, especially for craters closer to ~3 km in diameter, the degradation state could be interpreted as indicating either a late Mansurian or an early Kuiperian age. In addition, it is often difficult to determine clearly if the craters have been deformed by the fault [*Xiao et al.*, 2013]. However, even if the small craters have been disturbed only by mass wasting down the scarp face, downslope movement of material may still have been triggered by slip on the faults. The discovery of small lobate scarps, less than 10 km in length and interpreted to be Kuiperian in age on the basis of expected rates of impact degradation of morphology, provides supporting evidence that lithospheric contraction on Mercury continued into the Kuiperian [*Watters et al.*, 2015a].

Synoptic views of age relations between lobate scarp segments and impact craters are given in Figures 5 and 6. In Figure 5, scarp segments are distinguished by the youngest craters they clearly deform. The symbols plotted constrain the age of most recent activity on the underlying thrust faults to be later than those of the impact-forming events and of course do not constrain the time of formation of those faults. What is apparent is that lobate scarp segments that deform Calorian craters are widely distributed across the planet. Fewer scarp segments deform Mansurian and Kuiperian craters, but those segments, too, have an essentially global distribution. In Figure 6, scarp segments are distinguished by the oldest undeformed craters by which

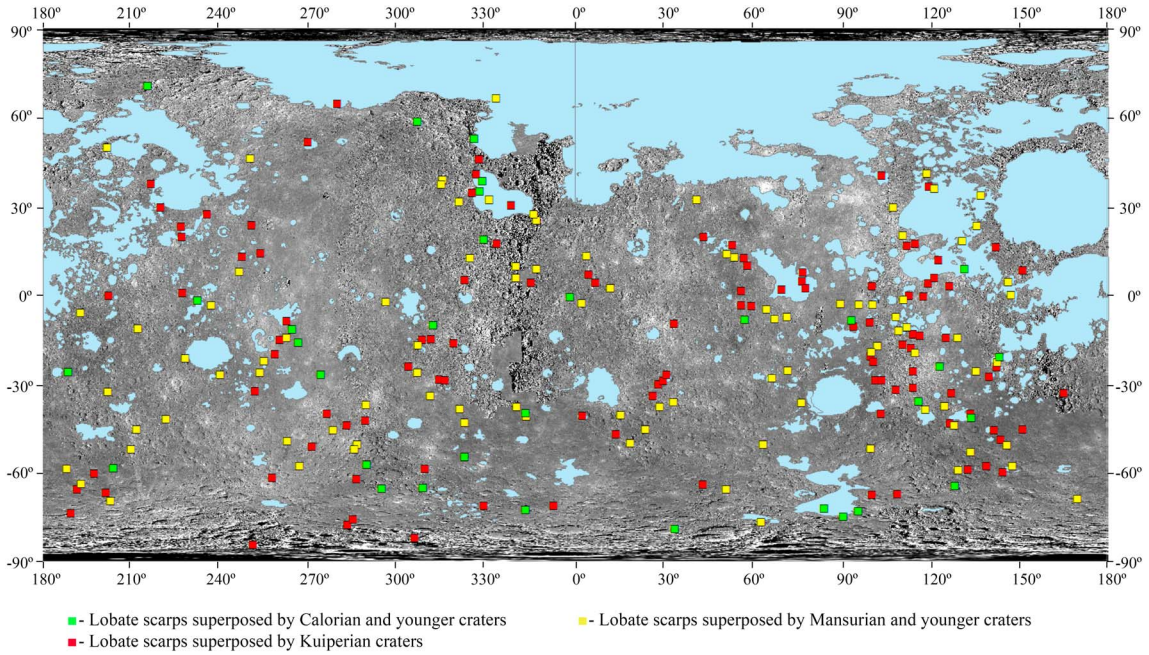

Figure 6. Locations of lobate scarp segments that coincide with impact craters, categorized by the oldest undeformed impact craters that superpose the scarps. Scarp segments superposed by Calorian and younger craters are represented by green squares, scarp segments superposed by Mansurian and younger craters by yellow squares, and scarp segments superposed by Kuiperian craters (rayed craters and relatively fresh craters <3 km in diameter) by red squares. Only examples of crosscutting relationships that could be clearly discerned in available images are included. The background image is an MDIS monochrome map in equirectangular projection. Smooth plains units [*Denevi et al.*, 2013] are shown in light blue.

they are superposed. The symbols plotted in this map constrain the age of the most recent detectable activity on the thrust faults associated with the scarp segments, and the time of formation of the fault and the initiation of slip, to before the crater-forming impact. Lobate scarp segments superposed by Kuiperian craters are widely distributed across the planet. Fewer, but still essentially globally distributed scarp segments, are superposed by Mansurian and Calorian craters. A notable exception to the above statements regarding geographic distribution is that few lobate scarp segments are seen on Mercury's smooth plains (Figures 5 and 6), where wrinkle ridges are the dominant contractional landforms [e.g., *Byrne et al.*, 2014; *Watters et al.*, 2015b].

In summary, the results of this study indicate evidence of activity on individual thrust fault segments during the Calorian, the Mansurian, and the Kuiperian systems. Thrust faulting has thus been a long-lived process through most of Mercury's history, initiating at least within the Calorian system, if not before (Figure 3c). The formation of the lobate scarps has been attributed primarily to long-term shortening of the lithosphere in response to cooling and contraction of the planetary interior [e.g., *Strom et al.*, 1975; *Watters et al.*, 1998; *Strom and Sprague*, 2003; *Solomon et al.*, 2008; *Watters and Nimmo*, 2010]. Other sources of compressive stress have no doubt played roles as well, and given the expected global uniformity and horizontal isotropy of stresses from interior contraction, these other sources influenced the distribution and orientations of the scarps. Additional sources of stress suggested to promote the formation or influence the location or orientation of thrust faults include tidal despinning, reorientation of the poles, mantle convective tractions, and lateral variations in topography and crustal thickness [*Strom et al.*, 1975; *Solomon*, 1979; *Pechmann and Melosh*, 1979; *Melosh and McKinnon*, 1988; *Schubert et al.*, 1988; *Hauck et al.*, 2004; *Watters et al.*, 2004, 2015b; *Dombard and Hauck*, 2008; *Matsuyama and Nimmo*, 2009; *Beuthe*, 2010; *Byrne et al.*, 2014; *Selvans et al.*, 2014; *Klimczak et al.*, 2015; *James et al.*, 2015]. All of these processes also predict extensional stress states at other locations on the planet, however, so the near-ubiquity of contractional landforms outside of the interiors of some volcanically infilled impact craters and basins implies that global contraction driven by interior cooling has dominated Mercury's lithospheric stress state since the end of the LHB.

Many thermal evolution models for Mercury [*Hauck et al.*, 2004; *Michel et al.*, 2013; *Tosi et al.*, 2013] predict that global contraction on Mercury began near or prior to the end of the LHB and continued to the present.

The findings of this study are consistent with and support these models. Calorian craters that are observed to superpose lobate scarps indicate that global contraction initiated during or before the Calorian system and near the end of emplacement of Mercury's youngest widespread smooth plains. Global contraction imposes a stress state on Mercury's lithosphere that serves to inhibit the ascent of magma to the surface [*Solomon*, 1978]. Indeed, crosscutting relations between lobate scarps and the youngest large expanses of smooth plains materials suggest that much of the activity on the associated thrust fault occurred after the most voluminous volcanism had ceased [e.g., *Watters et al.*, 2004, 2009b; *Denevi et al.*, 2013; *Byrne et al.*, 2015]. Nonetheless, smooth plains volcanism and contractional deformation likely overlapped for some period within the Calorian system [*Marchi et al.*, 2013; *Klimczak et al.*, 2013; *Byrne et al.*, 2015], and still younger smooth plains have been documented within the Rachmaninoff basin [*Prockter et al.*, 2010]. Moreover, MESSENGER orbital observations have revealed evidence for smaller features indicative of volcanism more recent than the time of emplacement of most smooth plains deposits, including irregular depressions interpreted as volcanic vents [*Denevi et al.*, 2013; *Rothery et al.*, 2014] and sources for pyroclastic deposits [*Kerber et al.*, 2009, 2011; *Goudge et al.*, 2013], as well as depressions formed by the withdrawal of magma from near-surface magma chambers [*Gillis-Davis et al.*, 2009; *Klimczak et al.*, 2013]. These younger volcanic features, however, are nearly all associated with impact craters, the formation of which served to remove the pre-existing stresses and would have permitted the ascent of mantle-derived magma even during an era dominated by global contraction. Some of these volcanic features are located in craters cut by thrust faults, but such faults could still have served as conduits for the vertical ascent of volatile-rich magmas [*Klimczak et al.*, 2013], such as those required to produce Mercury's largest pyroclastic deposits [*Kerber et al.*, 2009].

5. Conclusions

Observations of stratigraphic relations between lobate scarps and impact craters of different ages and states of degradation point to a prolonged interval of lithospheric shortening and thrust faulting on Mercury. That interval started within or before the Calorian system and extended through the Mansurian and into the Kuiperian systems. Global contraction resulting from interior cooling, the process primarily responsible for the majority of Mercury's contractional tectonic landforms, was thus a widespread and long-lived process that initiated at least near the end of the late heavy bombardment and continued over much of the last 3–4 Gyr. These findings are consistent with interior thermal evolution models that predict the onset of global contraction of Mercury near or prior to the end of the LHB and continuing contraction to the present [e.g., *Hauck et al.*, 2004; *Michel et al.*, 2013; *Tosi et al.*, 2013]. Additional analysis of images and data acquired by the MESSENGER spacecraft, especially higher-resolution images acquired during low-altitude operations late in the orbital mission, will provide further insights into the spatial and temporal distribution of tectonic activity on Mercury, as well as their implications for the planet's thermal and volcanic evolution.

Acknowledgments

We thank the entire MESSENGER team for their support of this investigation. We also thank Mark Robinson and two anonymous reviewers for helpful reviews of an earlier version of this manuscript. The MESSENGER project is supported by the NASA Discovery Program under contracts NASW-00002 to the Carnegie Institution of Washington and NAS5-97271 to The Johns Hopkins University Applied Physics Laboratory. This work was also supported by NASA grant NNX07AR60G. Data are available from the NASA Planetary Data System (https://pds.jpl.nasa.gov/).

References

Arthur, D. W. G., A. P. Agneray, R. A. Horvath, C. A. Wood, and C. R. Chapman (1963), The system of lunar craters, quadrant I, *Commun. Lunar Planet. Lab.*, *2*, 71–78.

Beuthe, M. (2010), East–west faults due to planetary contraction, *Icarus*, *209*, 795–817.

Braden, S. E., and M. S. Robinson (2013), Relative rates of optical maturation of regolith on Mercury and the Moon, *J. Geophys. Res. Planets*, *118*, 1903–1914, doi:10.1002/jgre.20143.

Byrne, P. K., C. Klimczak, A. M. C. Şengör, S. C. Solomon, T. R. Watters, and S. A. Hauck II (2014), Mercury's global contraction much greater than earlier estimates, *Nat. Geosci.*, *7*, 301–307.

Byrne, P. K., et al. (2015), Near-synchronous end to global-scale effusive volcanism on Mercury, *Lunar Planet. Sci.*, *46*, Abstract 1731.

Cintala, M. J. (1992), Impact-induced thermal effects in the lunar and mercurian regoliths, *J. Geophys. Res.*, *97*, 947–973, doi:10.1029/917JE0220.

Collins, G. S., H. J. Melosh, and B. A. Ivanov (2004), Modeling damage and deformation in impact simulations, *Meteorit. Planet. Sci.*, *39*, 217–231.

Denevi, B. W., and M. S. Robinson (2008), Mercury's albedo from Mariner 10: Implications for the presence of ferrous iron, *Icarus*, *197*, 239–246, doi:10.1016/j.icarus.2008.04.021.

Denevi, B. W., et al. (2013), The distribution and origin of smooth plains on Mercury, *J. Geophys. Res. Planets*, *118*, 891–907, doi:10.1002/jgre.20075.

Dombard, A. J., and S. A. Hauck II (2008), Despinning plus global contraction and the orientation of lobate scarps on Mercury, *Icarus*, *198*, 274–276.

Domingue, D. L., et al. (2014), Mercury's weather-beaten surface: Understanding Mercury in the context of lunar and asteroidal space weathering studies, *Space Sci. Rev.*, *181*, 121–214, doi:10.1007/s11214-014-0039-5.

Freed, A. M., S. C. Solomon, T. R. Watters, R. J. Phillips, and M. T. Zuber (2009), Could Pantheon Fossae be the result of the Apollodorus crater-forming impact within the Caloris basin, Mercury?, *Earth Planet. Sci. Lett.*, *285*, 320–327, doi:10.1016/j.epsl.2009.02.038.

Gault, D. E., J. E. Guest, J. B. Murray, D. Dzurisin, and M. C. Malin (1975), Some comparisons of impact craters on Mercury and the Moon, *J. Geophys. Res.*, *80*, 2444–2460, doi:10.1029/JB080i017p02444.

Gillis-Davis, J. J., D. T. Blewett, R. W. Gaskell, B. W. Denevi, M. S. Robinson, R. G. Strom, S. C. Solomon, and A. L. Sprague (2009), Pit-floor craters on Mercury: Evidence of near-surface igneous activity, *Earth Planet. Sci. Lett.*, *285*, 243–250, doi:10.1016/j.epsl.2009.05.023.

Goudge, T. A., et al. (2013), Global inventory and characterization of pyroclastic deposits on Mercury: New insights into pyroclastic activity from MESSENGER orbital data, *J. Geophys. Res. Planets*, *119*, 635–658, doi:10.1002/2013JE004480.

Hauck, S. A., II, A. J. Dombard, R. J. Phillips, and S. C. Solomon (2004), Internal and tectonic evolution of Mercury, *Earth Planet. Sci. Lett.*, *222*, 713–728, doi:10.1016/j.epsl.2004.03.037.

Hawkins, S. E., III, et al. (2007), The Mercury Dual Imaging System on the MESSENGER spacecraft, *Space Sci. Rev.*, *131*, 247–338.

James, P. B., M. T. Zuber, R. J. Phillips, and S. C. Solomon (2015), Support of long-wavelength topography on Mercury inferred from MESSENGER measurements of gravity and topography, *J. Geophys. Res. Planets*, *120*, 287–310, doi:10.1002/2014JE004713.

Kerber, L., J. W. Head, S. C. Solomon, S. L. Murchie, D. T. Blewett, and L. Wilson (2009), Explosive volcanic eruptions on Mercury: Eruption conditions, magma volatile content, and implications for interior volatile abundances, *Earth Planet. Sci. Lett.*, *285*, 263–271, doi:10.1016/j.epsl.2009.04.037.

Kerber, L., J. W. Head, D. T. Blewett, S. C. Solomon, L. Wilson, S. L. Murchie, M. S. Robinson, B. W. Denevi, and D. L. Domingue (2011), The global distribution of pyroclastic deposits on Mercury: The view from MESSENGER flybys 1–3, *Planet. Space Sci.*, *59*, 1895–1909, doi:10.1016/j.pss.2011.03.020.

Klimczak, C., P. K. Byrne, S. C. Solomon, F. Nimmo, T. R. Watters, B. W. Denevi, C. M. Ernst, and M. E. Banks (2013), The role of thrust faults as conduits for volatiles on Mercury, *Lunar Planet. Sci.*, *44*, Abstract 1390.

Klimczak, C., P. K. Byrne, and S. C. Solomon (2015), A rock-mechanical assessment of Mercury's global tectonic fabric, *Earth Planet. Sci. Lett.*, *416*, 82–90.

Kreslavsky, M. A., J. W. Head, G. A. Neumann, M. T. Zuber, and D. E. Smith (2014), Kilometer scale topographic roughness of Mercury: Correlation with geologic features and units, *Geophys. Res. Lett*, *41*, 8245–8251, doi:10.1002/2014GL062162.

Le Feuvre, M., and M. A. Wieczorek (2011), Nonuniform cratering of the Moon and a revised crater chronology of the inner Solar System, *Icarus*, *214*, 1–20, doi:10.1016/j.icarus.2011.03.010.

Leake, M. A. (1982), The intercrater plains of Mercury and the Moon: Their nature, origin, and role in terrestrial planet evolution, in *Advances in Planetary Geology*, *Tech. Memo. TM-84894*, pp. 3–535, NASA, Washington, D. C.

Marchi, S., S. Mottola, G. Cremonese, M. Massironi, and E. Martellato (2009), A new chronology for the Moon and Mercury, *Astrophys. J.*, *137*, 4936–4948.

Marchi, S., C. R. Chapman, C. I. Fassett, J. W. Head, W. F. Bottke, and R. G. Strom (2013), Global resurfacing of Mercury 4.0–4.1 billion years ago by heavy bombardment and volcanism, *Nature*, *499*, 59–61, doi:10.1038/nature12280.

Matsuyama, I., and F. Nimmo (2009), Gravity and tectonic patterns of Mercury: Effect of tidal deformation, spin-orbit resonance, nonzero eccentricity, despinning, and reorientation, *J. Geophys. Res.*, *114*, E01010, doi:10.1029/2008JE003252.

Melosh, J. H., and W. B. McKinnon (1988), The tectonics of Mercury, in *Mercury*, edited by F. Vilas, C. R. Chapman, and M. S. Matthews, pp. 374–400, Univ. of Arizona Press, Tucson, Ariz.

Michel, N. C., S. A. Hauck II, S. C. Solomon, R. J. Phillips, J. H. Roberts, and M. T. Zuber (2013), Thermal evolution of Mercury as constrained by MESSENGER observations, *J. Geophys. Res. Planets*, *118*, 1033–1044, doi:10.1002/jgre.20049.

Moore, H. J., J. M. Boyce, and D. A. Hahn (1980), Small impact craters in the lunar regolith – Their morphologies relative ages and rates of formation, *Moon Planets*, *23*, 231–252.

Pechmann, J. B., and H. J. Melosh (1979), Global fracture patterns of a despun planet: Application to Mercury, *Icarus*, *38*, 243–250.

Pohn, H. A., and T. W. Offield (1970), Lunar and crater morphology and the relative age determination of lunar geologic units. Part I. Classification, in *Geological Survey Research 1970*, *U.S. Geol. Surv. Prof. Pap.*, 700-C, pp. 153–162.

Prockter, L. M., et al. (2010), Evidence for young volcanism on Mercury from the third MESSENGER flyby, *Science*, *329*, 668–671.

Rothery, D. A., R. J. Thomas, and L. Kerber (2014), Prolonged eruptive history of a compound volcano on Mercury: Volcanic and tectonic implications, *Earth Planet. Sci. Lett.*, *385*, 59–67.

Schubert, G., M. N. Ross, D. J. Stevenson, and T. Spohn (1988), Mercury's thermal history and the generation of its magnetic field, in *Mercury*, edited by F. Vilas, C. R. Chapman, and M. S. Matthews, pp. 429–460, Univ. of Arizona Press, Tucson, Ariz.

Scott, D. H. (1977), Moon–Mercury: Relative preservation states of secondary craters, *Phys. Earth Planet. Inter.*, *15*, 173–178.

Selvans, M. M., T. R. Watters, P. B. James, and S. C. Solomon (2014), Statistical analysis of the distribution of tectonic features and crustal thickness in the northern hemisphere of Mercury, *Lunar Planet. Sci.*, *45*, Abstract 1442.

Senft, L. E., and S. T. Stewart (2007), Modeling impact cratering in layered surfaces, *J. Geophys. Res.*, *112*, E11002, doi:10.1029/2007JE002894.

Shoemaker, E. M., and R. J. Hackman (1962), Stratigraphic basis for a lunar time scale, in *The Moon*, edited by Z. Kopal and Z. K. Mikhailov, pp. 277–339, Academic Press, New York.

Solomon, S. C. (1978), On volcanism and tectonics on one-plate planets, *Geophys. Res. Lett.*, *5*, 461–464, doi:10.1029/GL005i006p00461.

Solomon, S. C. (1979), Formation, history and energetics of cores in the terrestrial planets, *Phys. Earth Planet. Inter.*, *19*, 168–182.

Solomon, S. C., et al. (2008), Return to Mercury: A global perspective on MESSENGER's first Mercury flyby, *Science*, *321*, 59–62, doi:10.1126/science.1159706.

Spudis, P. D., and J. E. Guest (1988), Stratigraphy and geologic history of Mercury, in *Mercury*, edited by F. Vilas, C. R. Chapman, and M. S. Matthews, pp. 118–164, Univ. of Ariz. Press, Tucson.

Stöffler, D., and G. Ryder (2001), Stratigraphy and isotope ages of lunar geologic units: Chronological standard for the inner solar system, *Space Sci. Rev.*, *96*, 9–54.

Strom, R. G., and A. L. Sprague (2003), *Exploring Mercury: The Iron Planet*, 216 pp., Springer Praxis Books, Chichester, U. K.

Strom, R. G., N. J. Trask, and J. E. Guest (1975), Tectonism and volcanism on Mercury, *J. Geophys. Res.*, *80*, 2478–2507, doi:10.1029/JB080i017p02478.

Strom, R. G., R. Malhotra, T. Ito, F. Yoshida, and D. A. Kring (2005), The origin of planetary impactors in the inner solar system, *Science*, *309*, 1847–1850, doi:10.1126/science.1113544.

Tosi, N., M. Grott, A.-C. Plesa, and D. Breuer (2013), Thermochemical evolution of Mercury's interior, *J. Geophys. Res. Planets*, *118*, 2474–2487, doi:10.1002/jgre.20168.

Trask, N. J. (1971), Geologic comparison of mare materials in the lunar equatorial belt, including Apollo 11 and Apollo 12 landing sites, *U.S. Geol. Surv. Prof. Pap.*, *750D*, 2645–2662.

Trask, N. J. (1975), Cratering history of the heavily cratered terrain on Mercury, *Proc. Int. Colloq. Planet. Geol., Geol. Rom*, *15*, 471–476.

Watters, T. R., and F. Nimmo (2010), The tectonics of Mercury, in *Planetary Tectonics*, edited by T. R. Watters and R. A. Schultz, pp. 15–80, Cambridge Univ. Press, New York.

Watters, T. R., M. S. Robinson, and A. C. Cook (1998), Topography of lobate scarps on Mercury: New constraints on the planet's contraction, *Geology*, *26*, 991–994.

Watters, T. R., R. A. Schultz, M. S. Robinson, and A. C. Cook (2002), The mechanical and thermal structure of Mercury's early lithosphere, *Geophys. Res. Lett.*, *29*, 1542, doi:10.1029/2001GL014308.

Watters, T. R., M. S. Robinson, C. R. Bina, and P. D. Spudis (2004), Thrust faults and the global contraction of Mercury, *Geophys. Res. Lett.*, *31*, L04071, doi:10.1029/2003GL019171.

Watters, T. R., S. L. Murchie, M. S. Robinson, S. C. Solomon, B. W. Denevi, S. L. André, and J. W. Head (2009a), Emplacement and tectonic deformation of smooth plains in the Caloris basin, Mercury, *Earth Planet. Sci. Lett.*, *285*, 309–319, doi:10.1016/j.epsl.2009.03.040.

Watters, T. R., S. C. Solomon, M. S. Robinson, J. W. Head, S. L. André, S. A. Hauck II, and S. L. Murchie (2009b), The tectonics of Mercury: The view after MESSENGER's first flyby, *Earth Planet. Sci. Lett.*, *285*, 283–296, doi:10.1016/j.epsl.2009.01.025.

Watters, T. R., et al. (2013), Distribution of prominent lobate scarps on Mercury: Contribution to global radial contraction, *Lunar Planet. Sci.*, *44*, Abstract 2213.

Watters, T. R., et al. (2015a), Small thrust fault scarps on Mercury revealed in low-altitude MESSENGER images, *Lunar Planet. Sci.*, *46*, Abstract 2240.

Watters, T. R., M. Selvans, M. E. Banks, S. A. Hauck II, K. J. Becker, and M. S. Robinson (2015b), Distribution of large-scale contractional tectonic landforms on Mercury: Implications for the origin of global stresses, *Geophys. Res. Lett.*, *42*, 3755–3763, doi:10.1002/2015GL063570.

Xiao, Z., et al. (2012), The youngest geologic terrains on Mercury, *Lunar Planet. Sci.*, *43*, Abstract 2143.

Xiao, Z., Z. Zeng, N. Ding, and J. Molaro (2013), Mass wasting features on the Moon - How active is the lunar surface?, *Earth Planet. Sci. Lett.*, *376*, 1–11.

Xiao, Z., R. G. Strom, C. R. Chapman, J. W. Head, C. Klimczak, L. R. Ostrach, J. Helbert, and P. D'Incecco (2014), Comparisons of fresh complex impact craters on Mercury and the Moon: Implications for controlling factors in impact excavation processes, *Icarus*, *228*, 260–275, doi:10.1016/j.icarus.2013.10.002.